IEEE Access
Multidisciplinary : Rapid Review : Open Access Journal

Received January 28, 2020, accepted February 10, 2020, date of publication February 21, 2020, date of current version March 18, 2020.

Digital Object Identifier 10.1109/ACCESS.2020.2975590

Experimental Investigation on Synchronization of Two Co-Rating Rotors Coupled With Nonlinear Springs

MINGJUN DU[1], YONGJUN HOU[1], CHENG YU[2], WEI WANG[1], DUYU HOU[1], AND GUANG XIONG[1]

[1]School of Mechatronics Engineering, Southwest Petroleum University, Chengdu 610500, China
[2]School of Intelligent Manufacturing, Chengdu Technological University, Chengdu 611730, China

Corresponding author: Mingjun Du (dmj9213@163.com)

This work was supported in part by the Sichuan Science and Technology Program under Grant 2018RZ0101, and in part by the Sichuan Science and Technology Program under Grant 2019YFG0317.

ABSTRACT This work is a continuation and verification of the original literature by using experimental strategy. Based on the published paper, in order to avoid anti-phase synchronization with two co-rotating rotors system, a vibrating system with two co-rotating rotors installed with nonlinear springs have been proposed, and then, the synchronous condition and the synchronous criterion of the system are theoretically derived. From the analysis mentioned, it is shown that the synchronous state is mainly determined by the structural parameters of the coupling unit, coupling coefficients and positional parameters of the two exciters, etc. The main objective of the present work is to investigate the synchronous mechanism by experiments and simulations in this paper. Some simulation computations are firstly implemented to explain the synchronous mechanism of the system. Additionally, an experimental strategy with synchronous tests and dynamic characteristic tests of the vibrating system are carried out to validate the correctness of the simulation analysis. The simulations and experiments demonstrate that the nonlinear springs can overcome the difference of residual torques of the two motors to realize the synchronization of near zero phase difference under the condition of in-phase difference between two exciters. Finally, the error analysis results among the dynamic testing, synchronous testing results and simulations are discussed. This research can provide theoretical reference for designing large-sized and heavy-duty Vibrating Screens.

INDEX TERMS Experimental strategy, synchronous condition, synchronous criterion, vibrating screens.

I. INTRODUCTION

Vibration utilization plays significant role in many fields of mechanical application. The most important representative of that is synchronization phenomena, which has already widely used in engineering applications. As one of the most conventional solids control systems, the vibrating screen plays a very important role in drilling fluid recovery. And the primary task is to remove a great deal of particles in drilling fluids by using the principle of ‘‘Vibration Synchronization’’. The study of the vibrating screen characteristic has drawn the attention of an increasing number of researchers who found the factors influencing the synchronism and stability, and those studies are mainly focusing on synchronization of two or multiple exciters. Blekhman firstly proposed synchronization theory of dynamic systems in 1950, and he explained the physical mechanism of a typical dual-motor excitation based on Pioncare–Laypunov method [1], [2]. Subsequently, Wen *et al.* proposed small parameter averaging method to investigate the synchronization of multiple rotors in after-resonance, and a lot of self-synchronous vibrating machines were invented at that time [3], [4]. Based on that, the average method of modified small parameters was described by Zhao, which has greatly simplified the process for solving the synchronous problems of multiple rotors, and he used it to investigate the dynamic characteristics of two exciters in a non-resonant vibrating system of plane motion [5]. Zhang *et al.* investigated the synchronization of three coupled exciters rotating with the same directions in a far-resonant vibrating system, and

The associate editor coordinating the review of this manuscript and approving it for publication was Jesus Felez.

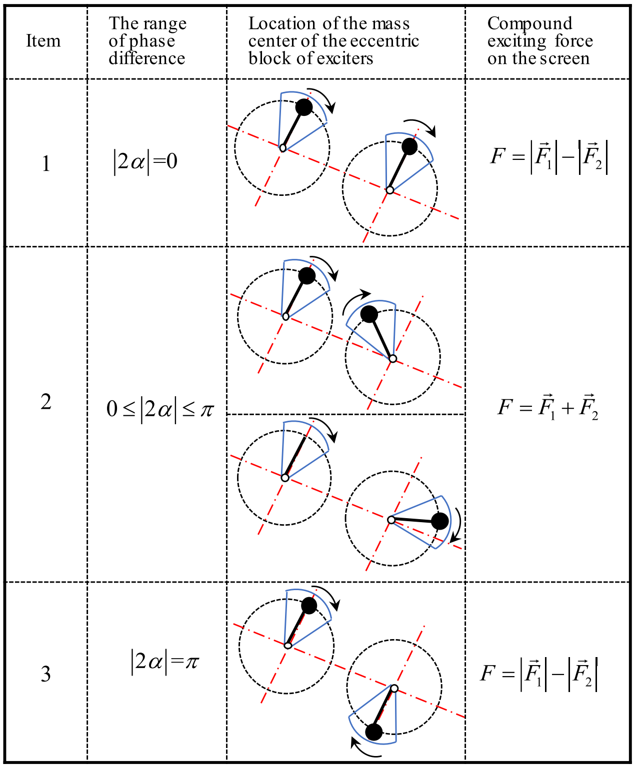

FIGURE 1. Relation between the phase difference of two exciters and compound exciting force on the screen.

the synchronization criterion and the stability criterion of the vibrating system are deduced [6]–[9]. In recent years, as vibration synchronization and the controlled synchronization have been widely used in mechanical engineering, Kong *et al.* used the master-slave control strategy to design a speed controller and phase difference controller by the sliding mode control and proportional–integral control methods [10]–[12]. Chen *et al.* studied the synchronization of two eccentric rotors with common rotational axis by applying the average method of small parameters, and he found that the vibration system has two steady motion modes [13]–[15]. Fang *et al.* proposed a Rotor-Pendulum System with the Multi-DOF Vibration, and the Poincare method was employed to study the synchronization characteristics of the system in a far-resonant vibrating system. It is indicated that the stiffness of the support spring, the stiffness of the connecting spring and the installation location of the motors affect the synchronous state of the system [16]–[18].

However, for synchronization of two exciters rotating with the same direction, the relationships between the phase difference of two exciters (2α) and compound exciting force on the screen $\left(\vec{\mathbf{F}}\right)$ are shown in Figure 1. It's easy to see that the resultant force exerted by two exciters is the maximum magnitude when $2\alpha = 0$. Conversely, the resultant force $\vec{\mathbf{F}}$ has a minimum magnitude when $2\alpha = \pi$. But in practical engineering applications, the two co-rotating eccentric rotors in the multi-motor driving system are easy to implement antiphase synchronization, which makes two exciting forces acting on the vibrating system neutralize each other. To meet the requirements of the strongly exciting force in engineering, the phase difference of two co-rotating eccentric rotors is expected to stabilize around zero. A mechanical model of two co-rating rotors coupled with nonlinear springs is proposed to implement in-phase synchronization. It is indicated that the effect of nonlinear springs is one of the main factors in the research of synchronous state and the stability criterion of the system. There is a clearance between two nonlinear serial springs, which makes the synchronization of the vibrating system lie in an uncertain state. Based on literature [19], this paper will provide the experimentally testing results to verify the correctness of the theoretical and numerical analysis. An experimental strategy with synchronous tests and dynamic characteristic tests of the vibrating system are constructed, and some experimental results and corresponding computer simulation are presented.

The article is structured as follows: The preface part of the article introduces the research background, the contents of the article and the research methods. In Sec. II, a mechanical model of two co-rating rotors coupled with nonlinear springs is described, and its synchronous condition and the synchronous stability are theoretically deduced by using the average method of modified small parameters. In Sec. III, Based on Runge–Kutta method, some computer simulations are performed to explain the synchronization principle. In Sec. IV, an experimental strategy with two co-rating rotors coupled with nonlinear springs are constructed, and those simulation results turns out to be correct by synchronous tests and dynamic characteristic tests. Additionally, error analysis about comparisons of the dynamic testing results, synchronous testing results and simulations results are given. Finally, some results are summarized in Sec. VI.

II. DYNAMIC MODEL AND THEORETICAL RESULTS

NOMENCLATURE

r_i	Eccentric radius of the exciter i, $r_1 = r_2 = r$, $i = 1, 2$
m_i	Mass of the exciter i, $i = 1, 2$
m_0	Mass of the vibrating body
M	Mass of the total vibration system, $M = m_0 + \sum_{i=1}^{2} m_i$
J_{oi}	Rotational inertia of the exciter i, $J_{oi} \approx m_i r_i^2$
J_0	Rotational inertia of the vibrating body
J	Rotational inertia of the vibrating system, $J = J_0 + \sum_{i=1}^{2} m_i l_i^2 + \sum_{i=1}^{2} m_i r_i^2$
k_j	Stiffness of supporting spring
f_j	Damping coefficient in j-direction
d_0	A clearance between two nonlinear serial springs
ℓ	Initial displacement between two exciters in x-direction, $\ell = \sqrt{l_1^2 + l_2^2 - 2l_1 l_2 \cos(\beta_2 - \beta_1)}$

l	Displace between the connection of each end of coupling unit at any time
l_i	Distance between the rotating center of the exciter i and the center of the system
β_i	Installation angle of the exciter i
T_c	Synchronous torque of frequency capture of the vibrating system
T_D	Difference of the residual torque of two exciters
T_{Ri}	Residual torque of the exciter i
L_{mk}	Mutual inductance of the exciter k
n_p	Pole-pairs
R_{rk}	Stator resistance of the exciter k
ω_{nj}	Natural frequency of the vibrating system in j-direction, $j = x, y, \psi$, $\omega_{nx} = \sqrt{k_x}/M$, $\omega_{ny} = \sqrt{k_y}/M$, $\omega_{n\psi} = \sqrt{k_\psi}/J$
ς_j	Damping factor of the vibrating system in j-direction, $\varsigma_x = f_x\big/(2\omega_{nx}M)$, $\varsigma_y = f_y\big/(2\omega_{ny}M)$, $\varsigma_\psi = f_\psi\big/(2\omega_{n\psi}J)$
n_j	Frequency ratio in j-direction, $n_x = \frac{\omega_m}{\omega_{nx}}$, $n_y = \frac{\omega_m}{\omega_{ny}}$, $n_\psi = \frac{\omega_m}{\omega_{n\psi}}$,
η_{12}	Mass ratio of the exciter 1 to the exciter 2, $\eta_{12} = \frac{m_1}{m_2}$
r_m, l_e, r_{li}	Dimensionless parameters $r_m = m_2\big/M$, $l_e = \sqrt{J\big/M}$, $r_{li} = l_i\big/l_e$
T_{e0i}	Driving torque of the exciter i
k_{ei}	Scaling factor of electrical and mechanical damping
ε_1	Instantaneous change coefficients of $\dot{\varphi}$, $\dot{\varphi} = (1+\varepsilon_1)\,\omega_m$
ε_2	Instantaneous change coefficients of $\dot{\alpha}$, $\dot{\alpha} = \varepsilon_2\omega_m$
ν_i	two new parameters, $\nu_1 = \varepsilon_1 + \varepsilon_2$, $\nu_2 = \varepsilon_1 - \varepsilon_2$
ω_m	Average angular velocity of two exciters over a period of time
2α	Phase differences between Exciter 1 and Exciter 2
φ	Average phase of two motors
γ_j	Lagging angle of phase of DOF $i(\bullet)$
W_{si}	Sine coefficient of the parameters $\gamma_j, j = x, y, \psi$
W_{ci}	Cosine coefficient of the parameters γ_j, $j = x, y, \psi$
U_{so}	Stator voltage
ω_s	Supply frequency of the power grid
L_{sk}	Stator inductance of the exciter k
$<\bar{\bullet}>$	Slow-changing parameters integrating over one period of time, $<\bar{\bullet}> = \frac{1}{T_0}\int_0^{T_0}(\bullet)dt$
$(\dot{\bullet})$	The first derivative of time, $d(\bullet)/dt$
$(\ddot{\bullet})$	The second derivative of time, $d^2(\bullet)/dt^2$

Figure 2 shows the nonlinear dynamic model of the vibrating system which consists of a body with mass m_0 placed on the foundation by four supporting springs with stiffness k_j and damping f_j in j-directions ($j = x, y, \psi$). Two exciters rotating in the same direction are parallelly mounted on the

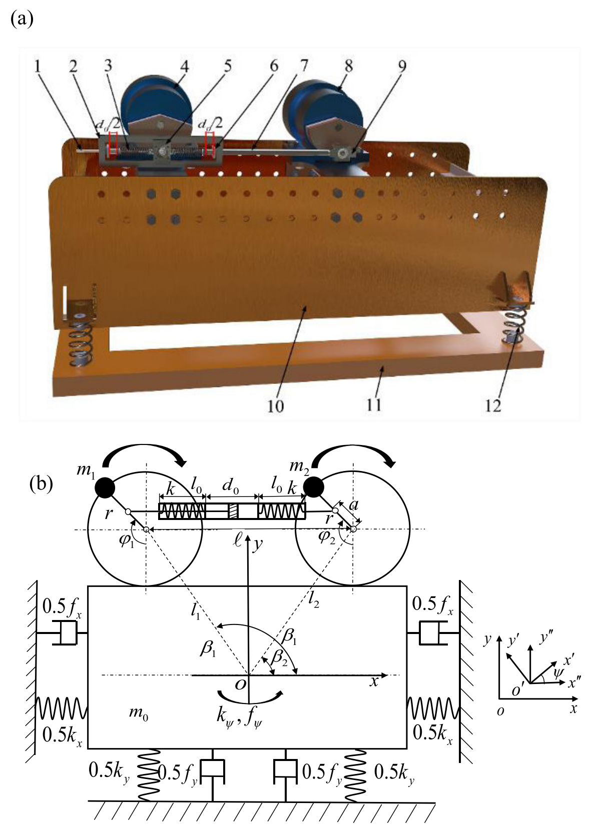

FIGURE 2. Vibrating system with two co-rating rotors coupled with nonlinear springs: (a) 3D model; (b) Dynamic model. 1. The guiding rod; 2. Bounding box; 3. compression springs; 4. The 1th exciter; 5. sliding block; 6. Locknut; 7. The connecting rod; 8. The 2th exciter; 9. sliding block; 10. vibrating body; 11. Foundation; 12. supporting springs.

vibrating body via the motor seat, which are connected with a coupling unit. The coupling unit consists of two springs in serial, connecting rod, guiding rod, bounding box, sliding block and locknut. The spring has zero mass, spring constant k, unstretched length l_0[m] and there exists an interstice d_0[m] between the two compression springs, which may cause severe nonlinear behaviors. Considering two exciters are simplified as a material point m_i with rotating radius r_i, as shown in Fig.1(b). The motion of the vibrating body is assumed to be confined to the plane oxy, where exhibits three degrees of freedom along x, y and ψ directions, respectively. According to [19] and the general form of Lagrange's equation, the dynamic equations of the vibrating system are derived as follows:

$$M\ddot{x} + f_x\dot{x} + k_x x = \sum_{i=1}^{2} m_i r_i \left(\ddot{\varphi}_i \cos\varphi_i - \dot{\varphi}_i^2 \sin\varphi_i\right)$$

$$M\ddot{y} + f_y\dot{y} + k_y y = -\sum_{i=1}^{2} m_i r_i \left(\ddot{\varphi}_i \sin\varphi_i + \dot{\varphi}_i^2 \cos\varphi_i\right)$$

$$J\ddot{\psi} + f_\psi\dot{\psi} + k_\psi \psi = \sum_{i=1}^{2} m_i l_i r_i \begin{bmatrix} \ddot{\varphi}_i \sin(\varphi_i + \beta_i) \\ +\dot{\varphi}_i^2 \cos(\varphi_i + \beta_i) \end{bmatrix}$$

$$
\begin{aligned}
J_{o1}\ddot{\varphi}_1 + f_1\dot{\varphi}_1 &= M_{e1} - R_{e1} + m_1 r_1[\ddot{x}\cos(\varphi_1+\psi) \\
&\quad - \ddot{y}\sin(\varphi_1+\psi) + l_1\ddot{\psi}\sin(\varphi_1+\beta_1) \\
&\quad - l_1\dot{\psi}^2\cos(\varphi_1+\beta_1)] - ka^2(\sin\varphi_1 \\
&\quad - \sin\varphi_2)\cos\varphi_1 \\
J_{o2}\ddot{\varphi}_2 + f_2\dot{\varphi}_2 &= M_{e2} - R_{e2} + m_2 r_2[\ddot{x}\cos(\varphi_2+\psi) \\
&\quad - \ddot{y}\sin(\varphi_2+\psi) + \ddot{\psi} l_2\sin(\varphi_2+\beta_2) \\
&\quad - \dot{\psi}^2 l_2\cos(\varphi_2+\beta_2)] + ka^2(\sin\varphi_1 \\
&\quad - \sin\varphi_2)\cos\varphi_2 \qquad (1)
\end{aligned}
$$

where

$$
k = \begin{cases} c & (0 \le l - \ell - 0.5d_0 \le l_0) \\ & \cup (0 \le \ell - l - 0.5d_0 \le l_0) \\ 0 & \text{other} \end{cases}
$$

Blekhman has put forward that the change of average angular velocity $\dot{\varphi}$ with two exciters is slow-changing parameter [2]. As synchronous behavior of vibrating system gradually occurs, its value $\dot{\varphi}$ in terms of time is approximately a constant ω_m. In light of the average method of modified small parameters, discarding higher-order terms of small parameters ν_i $(i = 1, 2)$, the dimensionless coupling equation of the system can be expressed as follows [19]:

$$
\mathbf{A}\dot{\mathbf{v}} = \mathbf{B}\boldsymbol{\nu} + \boldsymbol{\mu} \qquad (2)
$$

where

$$
\mathbf{v} = [\bar{\nu}_1, \bar{\nu}_2]^T, \quad \boldsymbol{\mu} = [\mu_1, \mu_2]^T, \ \mathbf{A} = \begin{bmatrix} a_{11} & a_{12} \\ a_{21} & a_{22} \end{bmatrix},
$$

$$
\mathbf{B} = \begin{bmatrix} b_{11} & b_{12} \\ b_{21} & b_{22} \end{bmatrix}
$$

$$
\begin{aligned}
a_{11} &= \rho_1 + \frac{1}{2}W_s\cos(2\alpha-\theta_s) + \frac{1}{2}W_c\sin(2\alpha+\theta_c) \\
a_{12} &= \rho_2 + \frac{1}{2}W_s\cos(2\alpha-\theta_s) - \frac{1}{2}W_c\sin(2\alpha+\theta_c) \\
a_{21} &= \rho_1 - \frac{1}{2}W_s\cos(2\alpha-\theta_s) - \frac{1}{2}W_c\sin(2\alpha+\theta_c) \\
a_{22} &= -\rho_2 + \frac{1}{2}W_s\cos(2\alpha-\theta_s) - \frac{1}{2}W_c\sin(2\alpha+\theta_c) \\
b_{11} &= -\omega_m k_1 + \omega_m W_s\sin(2\alpha-\theta_s) - \omega_m W_c\cos(2\alpha+\theta_c) \\
b_{12} &= -\omega_m k_2 - \omega_m W_s\sin(2\alpha-\theta_s) - \omega_m W_c\cos(2\alpha+\theta_c) \\
b_{21} &= -\omega_m k_1 - \omega_m W_s\sin(2\alpha-\theta_s) + \omega_m W_c\cos(2\alpha+\theta_c) \\
b_{22} &= \omega_m k_2 - \omega_m W_s\sin(2\alpha-\theta_s) - \omega_m W_c\cos(2\alpha+\theta_c)
\end{aligned}
$$

The coefficients of the equation (2) are given in Appendix. The symbol $\mathbf{A}$ is inertial coupling matrix of two exciters, the symbol $\mathbf{B}$ is stiffness matrix of two exciters and the symbol $\boldsymbol{\mu}$ is coupling matrix of the driving torque and the resistance torque of two exciters. Where in the steady state, those slowly varying small parameters are approximately equal to zero. So $\bar{\nu}_1 = 0, \bar{\nu}_2 = 0$.

Rearranging $\bar{\nu}_1$ and $\bar{\nu}_2$, we obtain

$$
\begin{aligned}
&T_{e01} + T_{e02} - (f_1+f_2)\,\omega_m - \frac{1}{2}m_2 r^2\omega_m^2\left(\eta_{12}^2 W_{s1} + W_{s2}\right) \\
&\quad - m_2 r^2\omega_m^2 W_c\cos(2\alpha+\theta_c) = 0 \\
&(T_{e01} - T_{e02}) - \omega_m(f_1 - f_2) + \frac{1}{2}m_2 r^2\omega_m^2\left(W_{s2} - \eta_{12}^2 W_{s1}\right) \\
&\quad = m_2 r^2\omega_m^2 W_s\sin(2\alpha-\theta_s) + ka^2\sin(2\alpha) \qquad (3)
\end{aligned}
$$

We shall now recast difference equation of two exciters. And define a difference of residual torque of two exciters (T_D) and synchronous torque of frequency capture (T_c). Then we may rewrite the second equation(3) in terms of T_D and T_c:

$$
\frac{T_D}{T_c} = \sin(2\alpha - \theta_M) \qquad (4)
$$

where

$$
\begin{aligned}
T_D &= T_{R1} - T_{R2}, \\
T_c &= \sqrt{(m_2 r^2\omega_m^2 W_s\cos\theta_s + ka^2)^2 + (m_2 r^2\omega_m^2 W_s\sin\theta_s)^2} \\
T_{R1} &= T_{e01} - \omega_m f_1 - \frac{1}{2}m_2 r^2\omega_m^2\eta_{12}^2 W_{s1}, \\
T_{R2} &= T_{e02} - \omega_m f_2 - \frac{1}{2}m_2 r^2\omega_m^2 W_{s2} \\
\theta_M &= \begin{cases} \arctan\dfrac{m_2 r^2\omega_m^2 W_s\sin\theta_s}{m_2 r^2\omega_m^2 W_s\cos\theta_s + ka^2}, & m_2 r^2\omega_m^2 W_s\cos\theta_s + ka^2 \ge 0 \\ \pi + \arctan\dfrac{m_2 r^2\omega_m^2 W_s\sin\theta_s}{m_2 r^2\omega_m^2 W_s\cos\theta_s + ka^2}, & m_2 r^2\omega_m^2 W_s\cos\theta_s + ka^2 < 0 \end{cases}
\end{aligned}
$$

The synchronous condition implementing vibrating synchronization for two exciters can be expressed as:

$$
|T_D| \le T_c \qquad (5)
$$

According to Routh-Hurwitz, the stability criterion of synchronous states of the vibrating system is

$$
c_1 > 0, \quad c_3 > 0, \ c_1 c_2 > c_3 \qquad (6)
$$

where

$$
\begin{aligned}
c_1 &= 4\omega_m H_1/H_0, \quad c_2 = 2\omega_m^2 H_2/H_0, \ c_3 = 2\omega_m^3 H_3/H_0 \\
H_0 &= 4\rho_1\rho_2 - W_s^2\cos^2(2\alpha-\theta_s) + W_c^2\sin^2(2\alpha+\theta_c) \\
H_1 &= \rho_2 k_1 + \rho_1 k_2 - W_s W_c\cos(\theta_c+\theta_s) \\
H_2 &= 2k_1k_2 + W_s^2\sin^2(2\alpha-\theta_s) - W_c^2\cos^2(2\alpha+\theta_c) \\
&\quad + W_s^2 - W_c^2 + (\rho_1-\rho_2)\,W_c\sin(2\alpha+\theta_c) \\
&\quad + (\rho_1+\rho_2)\,W_s\cos(2\alpha-\theta_s) \\
&\quad + [(\rho_1+\rho_2) + W_s\cos(2\alpha-\theta_s)]\,\frac{ka^2}{m_2 r^2\omega_m^2}\cos(2\alpha) \\
H_3 &= (k_1+k_2)\,W_s\cos(2\alpha-\theta_s) \\
&\quad - (k_2-k_1)\,W_c\sin(2\alpha+\theta_c) + 2W_cW_s\cos(\theta_s+\theta_c) \\
&\quad + [k_1+k_2+2W_c\cos(2\alpha+\theta_c)]\,\frac{ka^2}{m_2 r^2\omega_m^2}\cos(2\alpha)
\end{aligned}
$$

III. SIMULATION ANALYSIS

The theoretical derivation with the dimensionless coupling torque balanced equations of two exciters and the stability criterion implementing vibrating synchronization are given in preceding section. The dynamic characteristics of the system for different structural parameters are discussed numerically

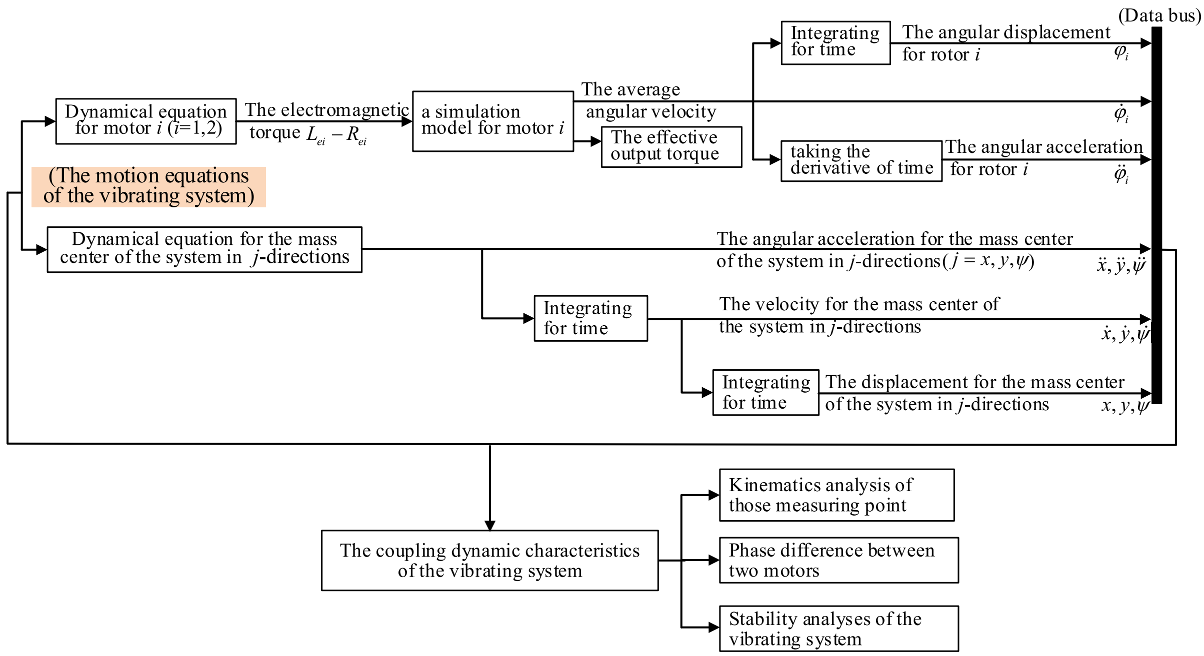

FIGURE 3. Schematic diagram of simulation model.

in literature [19]. From this investigation, it is found that the synchronization state of the system is influenced by the coupling unit, coupling coefficients, and positional parameters of two exciters, etc. When the vibrating system operates at the steady state, the electromagnetic torque and the stiffness coefficients can be expressed as follows [5]:

$$T_{ek} = n_p \frac{L_{mk} U_{so}^2}{L_{sk} \omega_s R_{rk}} (\omega_s - n_p \omega_m) \tag{7}$$

$$k_{ek} = n_p^2 \frac{L_{mk}^2 U_{so}^2}{L_{sk} \omega_s R_{rk}} \tag{8}$$

Considering that two exciters are identical with each other, we use the Runge–Kutta algorithm with adaptive control to establish the simulation model with two co-rating rotors coupled with nonlinear springs based on the motion equations (1). The schematic diagram of simulation of the system are shown in Figure 3, and it can be found that the coupling dynamic characteristics of the vibrating system consisting of kinematics analysis of those measuring point, the phase difference between two exciters and stability analysis are easily obtained. The structure parameters with two co-rating rotors coupled with nonlinear springs are given in Table 1.

Figure 4 presents results of computer simulation when $k = 0$. When two exciters are simultaneously supplied with the electric source, the vibrating system pass in the region of resonance after a short moment, which reach the synchronous operation state. As shown in Figure 4(a), the synchronous rotational velocity of both two exciters is 151.2 rad/s while five minutes later. The phase difference between the two exciters is stabilized at 3.03 rad in the steady state, as shown

TABLE 1. The structural parameters of the vibrating system.

Unbalanced rotors ($i = 1, 2$)	Vibrating body	Coupling unit	Induction motor
m_i =2[kg]	M =73.6[kg]	k =0 ~1×10^8 [N/m]	$\omega_x = 50$ [Hz]
r =0.04[m]	J =6.8[kg.m2]	a =0.02[m]	$U_{so} = 220$ [V]
ω_m =157[rad/s]	k_x =1.7×104 ~8×107[N/m]	d_0 =0~0.08[m]	$n_p = 2$
c_i =0.02[N.s/m]	k_y =1.7×104 ~8×107[N/m]	l_0 =0.04~0.07[m]	$R_{si} = 0.54$
l_1 =0.23[m]	k_ψ =1.6×103 ~1.7×107 [N/rad]	—	$L_m = 0.13$ [H]
l_2 =0.28 [m]	f_x =1000[N.s/m]	—	$L_r = 0.2$
$\beta_1 = 132^\circ$	f_y =1000[N.s/m]	—	$L_{sk} = 0.1$ [H]
$\beta_2 = 38^\circ$	f_ψ =1000[N.s/rad]	—	—

in Figure 4(b). Besides, the displacement responding of mass center of the system in $j - (j = x, y, \psi)$ directions are shown in Figure 4(c), (d) and (e), one can see that the vibrating system is oscillated periodically in the plane oxy.

Figure 5 shows results of computer simulation when setting $k = 82000$ N/m. The phase difference between the two exciters is stabilized at 0.013 rad while the vibrating system operates at the steady state. This phenomenon is mainly due to the existence of the coupling unit, and which guarantee the synchronous state locked in-phase synchronization state. The displacements of the vibrating body are shown in Figure 5(b), (c) and (d), and comparing with the results in Figure 4, it is demonstrated that the response amplitude of the vibrating system has remarkably improved.

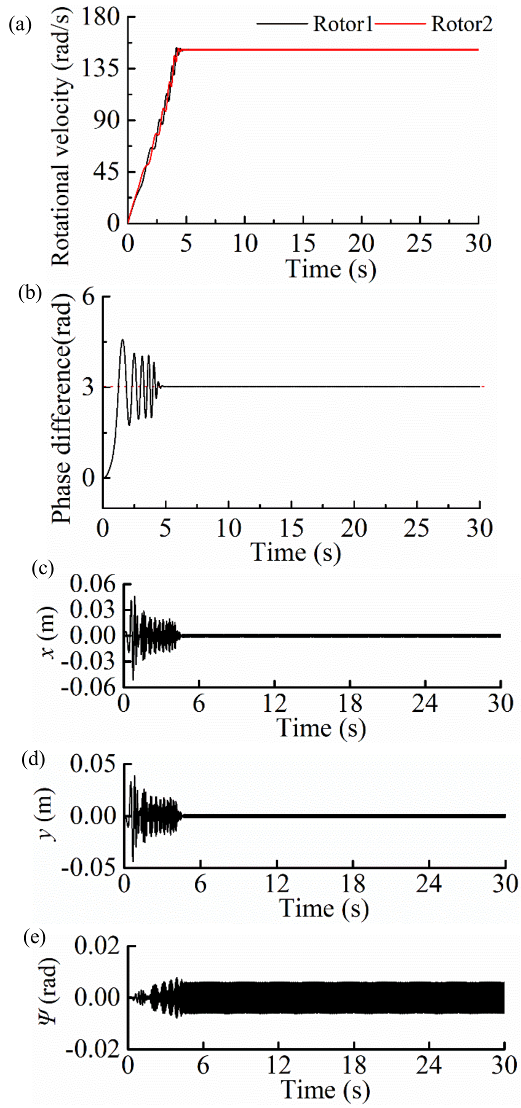

FIGURE 4. Results of computer simulation for: (a) Rotational velocity; (b) Phase difference between two rotors; (c) Response of mass center of the system in x-direction; (d) Response of mass center of the system in y-direction; (e) Response of mass center of the system in ψ-direction.

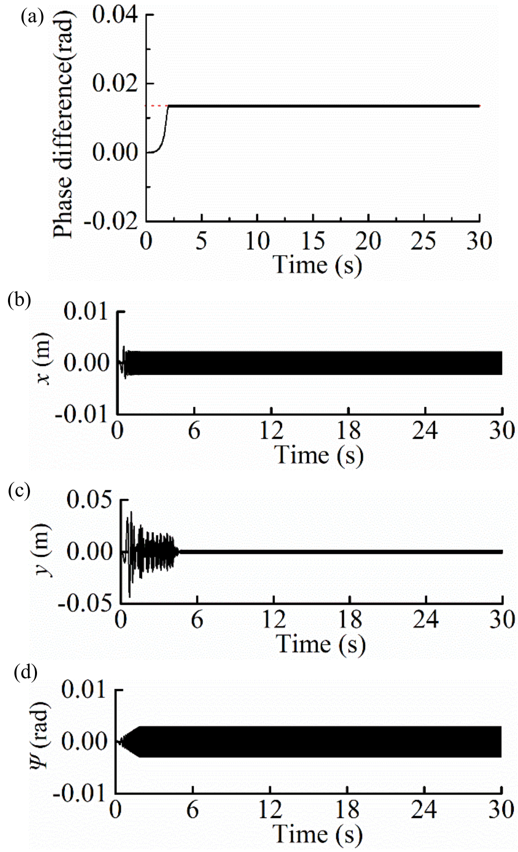

FIGURE 5. Results of computer simulation for: (a) Phase difference between two rotors; (b) Response of mass center of the system in x-direction; (c) Response of mass center of the system in y-direction; (d) Response of mass center of the system in ψ-direction.

IV. EXPERIMENTAL ANALYSIS

From the preceding simulation analysis, it can be seen that the steady phase difference between two rotors is influenced by the structural parameters of the coupling unit, coupling coefficients and positional parameters of two induction motors. To prove the correctness of the simulation analysis, an experimental strategy with synchronous tests and dynamic characteristic tests of the vibrating system are constructed in Figure 6. The testing system consists of an experimental prototype, high-speed imaging system and dynamic testing system.

High Resolution images can be captured in a very short exposure time (the speed of 100-2500000 frames per second) for an application like rotating object, and it can perform real-time codec processing and display for collected image data. As shown in Figure 7, a high-speed camera is employed to capture the transiently state of two rotors during synchronous process, MEMRECAM Hxlink (HX) software is applied to extract transient image of the system and a spotlight is used as a supplement to the brightness of the moving object.

The dynamic testing system consisting mainly of the piezoelectric acceleration sensor, the vibrating calibration for acceleration sensor, the vibrating analysis software (Coinv DASPV10) and the vibration measuring instrument (INV3060A) is shown in Figure 8. And which used mainly for signal acquisition, statistical analysis, time domain analysis, autocorrelation analysis, spectrum analysis, self-power spectrum analysis, etc. Through collecting and analyzing vibration signal in the frequency domain, the movement laws of those measuring point is presented with the vibrating analysis software.

The experimental prototypes that are composed of three vibration three-phase asynchronous motor (YZS-1.5-4), four supporting springs, a vibrating body, supporting springs, foundation, the coupling unit, etc., are shown in Figure 9. The vibration three-phase asynchronous motor consists of adjustable eccentric block at the ends of its rotational axis, the magnitude with the exciting force of the motor can be adjusted by changing between the eccentric the included angle. The motor performance parameters of YZS-1.5-4 are

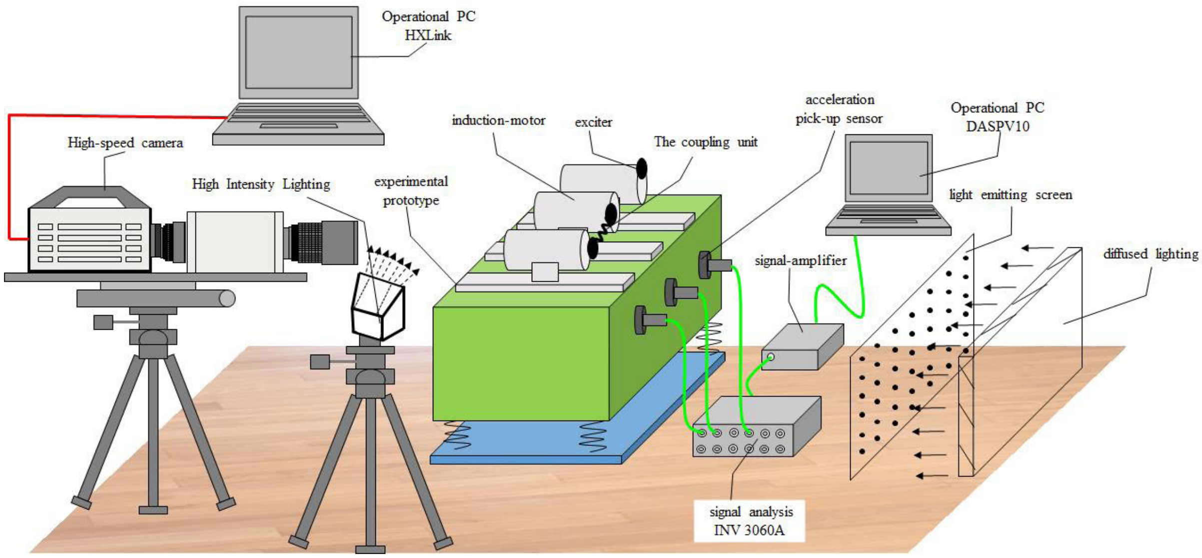

FIGURE 6. The dynamic testing scheme of nonlinear vibration system.

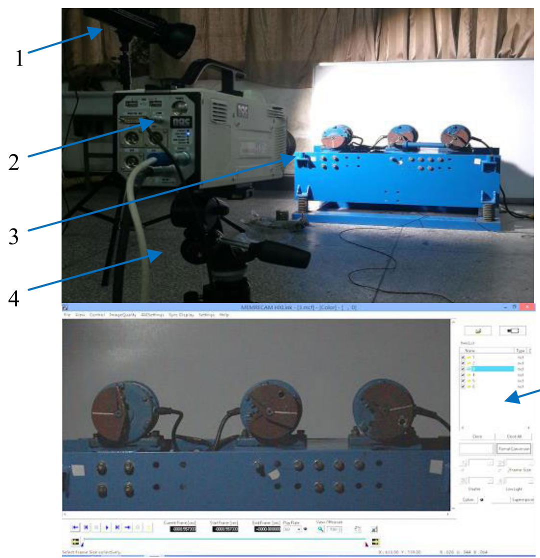

FIGURE 7. High-speed imaging system. 1. A spotlight; 2. High-speed camera (HX-6E); 3. Experimental prototype; 4. A tripod; 5. HX software.

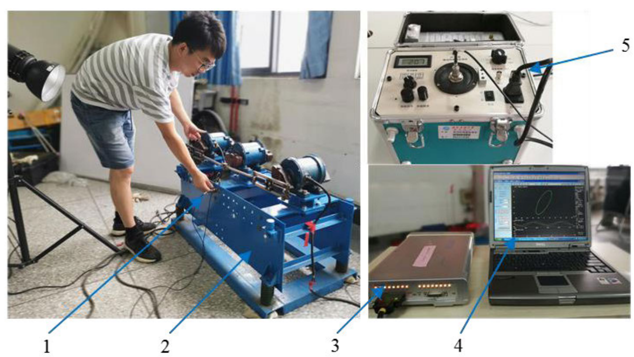

FIGURE 8. The dynamic testing Systems. 1. Acceleration pick-up sensor; 2. Experimental prototype. 3. Vibration measuring instrument (INV3060A); 4. Vibrating analysis software (Coinv DASPV10); 5. Calibrating instrument for sensor.

TABLE 2. Parameters for vibration three-phase asynchronous motor (YZS-1.5-4).

Parameter	Voltage [V]	Power rating [HZ]	Output Power [kw]	Current [A]	Frequency [r/min]	Exciting force [kN]	Weight [kg]
Value	380	50	0.12	0.36	1500	1.5	16

shown in Table 2. Three asynchronous motor are parallelly placed on the top of the vibrating body via the motor seat, and two adjacent exciters are connected with the coupling unit consisting of two springs in serial, connecting rod, guiding rod, bounding box, sliding block and locknut. During the process of synchronous operation, two springs in serial have always been subjecting to a changing force alternately in compression, and in-phase synchronization between the exciters rotating in the same directions is easy implemented.

Those measuring-point arrangement (P_1, P_2, P_3, P_4) for piezoelectric acceleration sensor are illustrated in Figure 9(a). and the relations between the any testing point in rigid frame and the mass center of the vibrating system are shown in Figure 10. xoy, $x'o'y'$ and $x''o'y''$ are the fixed frame, the non-rotating moving frame, the rotating frame, respectively. The mass center of the rigid frame is coincided with origin of the fixed frame xoy. The distances between the any testing point P and the center of mass of the rigid frame is described as op, and the angle between op and horizontal axis (the x-axis) is expressed by θ in the quiescent state. During the running process of the steady-state, the displacements of testing point (P') in rigid frame along the horizontal direction

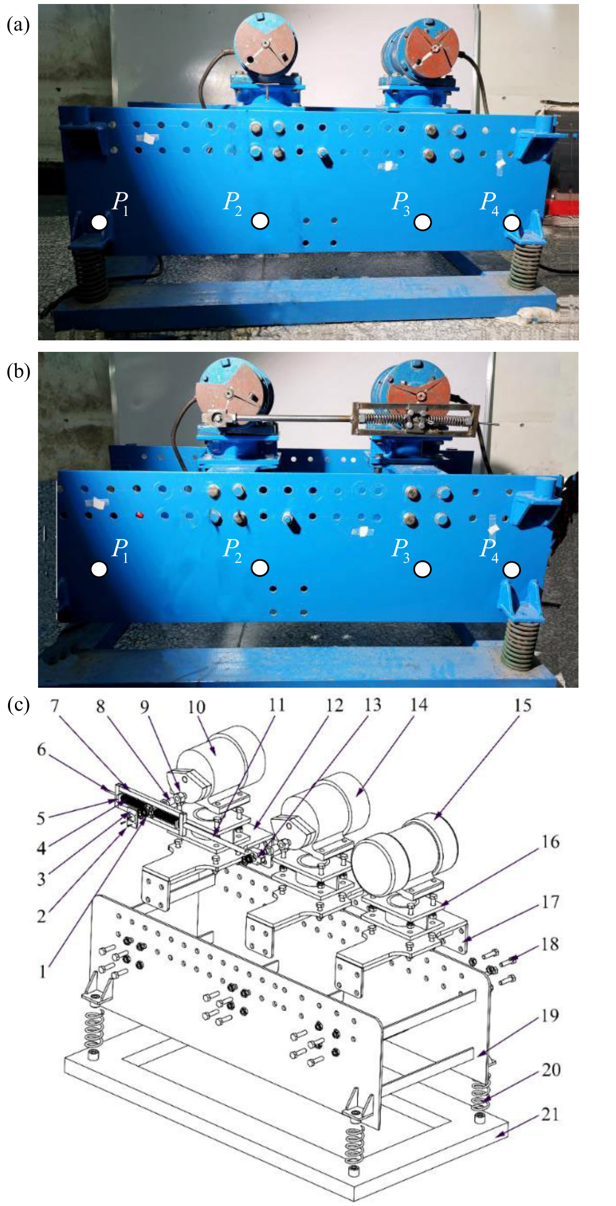

FIGURE 9. **The experimental prototypes: (a) two co-rotating rotors in a vibrating system; (b) two co-rotating rotors coupled with a tensile-spring in a vibrating system; (c) 3D model 1. Rolling bearing; 2. Locking bolts; 3. Limiting plate; 4. Compression spring; 5. Adjusting nut; 6. Guiding rod; 7. Bounding box; 8. The axis; 9. Locking bolt; 10. Induction motor 1; 11. Connecting rod; 12. Motor seat; 13. Sliding block; 14. Induction motor 2; 15. Induction motor 3; 16. Supporting foundation; 17. Motor base; 18. Bolt fastening; 19. Vibrating body; 20. Supporting springs; 21. Foundation.**

and the vertical direction are given by:

$$\begin{aligned} x_p &= x + op\cos(\theta+\psi) - op\cos\theta \\ y_p &= y + op\sin(\theta+\psi) - op\sin\theta \end{aligned} \tag{9}$$

The experimental prototypes with two co-rotating rotors in a vibrating system are shown in Figure 9. The primary parameters are $l_1 = 0.23$ m, $l_2 = 0.28$m, $\beta_1 = 132°$, $\beta_2 = 38°$. Other parameters are identical with Table 1. And the positional parameters of four measuring-point with

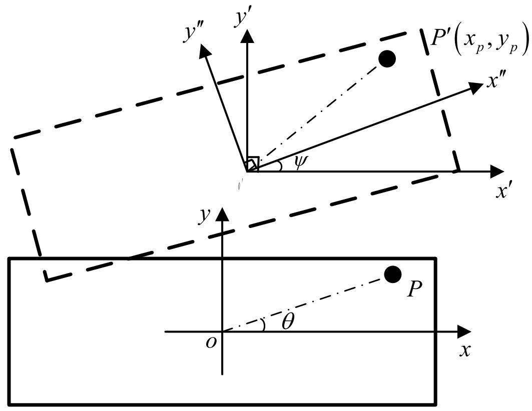

FIGURE 10. **Relations between the any testing point (*P* and *P′*) in rigid frame and the mass center (*O*) of the vibrating system.**

respect to mass center of the system are $P_1(-0.48\ ,-0.2)$, $P_2(-0.26\ ,-0.2)$, $P_3(0.19\ ,-0.2)$, $P_4(0.42\ ,-0.2)$, respectively. Figure 11(a) presents spectral analysis for point P_2 and P_3 along x-direction and y-direction. It is evident that the peak spectral occurs in horizontal and vertical directions when the vibrational frequency of the system is approximately equal to 28.125 Hz. Figure 11(b) and (c) shows the accelerations of four measuring-point along horizontal and vertical directions, then it is easily shown that those horizontal acceleration trend to be the same in the numerical value (the amplitude of acceleration is equal to 29 m/s^2). However, those vertical acceleration was different in the numerical value, the acceleration amplitude of four measuring-point are 44.7 m/s^2, 26.2 m/s^2, 21.1 m/s^2 and 37 m/s^2, respectively. Which result to the trajectory of four measuring-point are different (including the vibrating direction and the max amplitude of the measuring-point), as shown in Figure 11(j). Double integration algorithm is applied to the accelerations of four measuring-point to get its displacements in horizontal and vertical directions, as shown in Figure 11(f), (g), (h) and (i), respectively. And its magnitudes of dynamic testing are listed in Table3. In addition, an electromagnetic coupling model with two co-rotating rotors in a vibrating system are employed to obtain the displacement amplitudes of four measuring-point by computer simulations. And the simulation results with two co-rotating rotors in a vibrating system are shown in Table 3. Comparing with the results of the test data, the error of magnitudes of the measuring-point is within 30%, for the reason that the machining error of experimental prototypes, an asymmetric installation of two asynchronous motor, stiffness measuring errors of the springs, etc. The motion trajectories of any measuring-point in the rigid frame are nontranslational elliptically as the mass center and the center of force of the system don't coincide with each other, as shown in Figure 11(j).

As shown in Figure 12, the transiently state of two rotors in the operating process of system is obtained by the high-speed camera. It is evident that the instantaneous phase relationship of two exciters during the synchronous state, is nearly2.69 rad

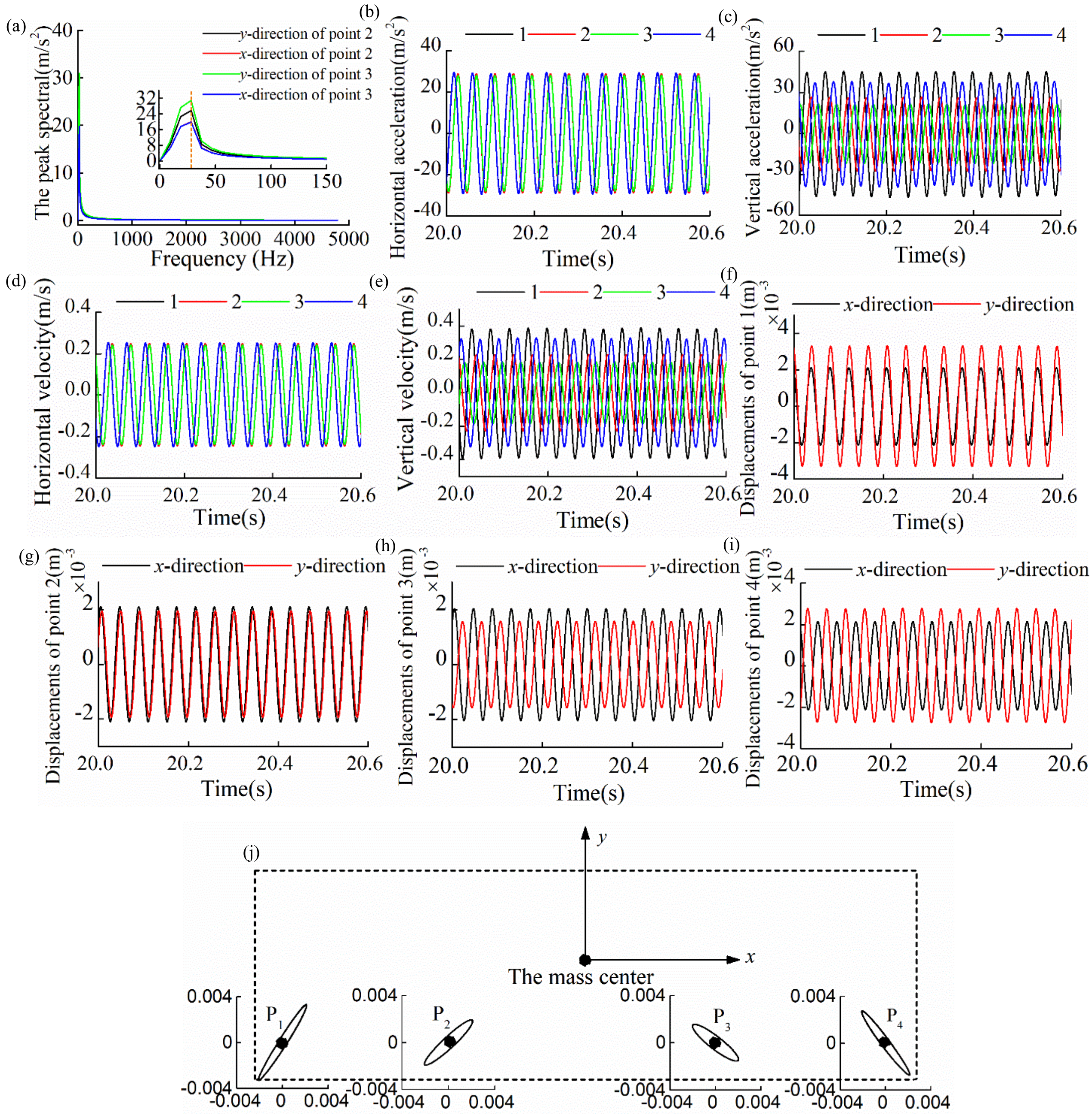

FIGURE 11. Testing results of dynamic characteristic with two co-rotating rotors in a vibrating system: (a) The spectral analysis; (b) Horizontal accelerations of the measuring point; (c) Vertical accelerations of the measuring point; (d) Horizontal velocity of the measuring point; (e) Vertical velocity of the measuring point; (f) Displacements of the point 1; (g) Displacements of the point 2; (h) Displacements of the point 3; (i) Displacements of the point 4; (j) Motion trail of the measuring point in *xoy* plane.

($-205.9° = 154.1° - 360°$). The simulation results of phase difference of two exciters were proven to be in good agreement with its testing result in Table 4 (the phase difference of two exciters in the simulation is close to 3.03[rad]), and the error is 11.2%.

Considering the model that two co-rotating rotors installed with two serial springs on which there is a clearance, the synchronizing characteristic of the system are given in Figure 13 and 14. It is shown that the vibrating system shows severe nonlinearities, and two exciters can't rotate with the same velocity. Eventually, this can lead to the displacements and the accelerations of point P_2 and P_3 appeared as marked non-periodic change in horizontal and vertical directions. One exciter is in good operation. And the other exciter is swing from side to side.

For two co-rotating rotors coupled with a tensile-spring in a vibrating system(Figure 9(b)), those testing results of dynamic characteristic are shown in Figure 15, and the

FIGURE 12. Phase difference with two co-rotating rotors in a vibrating system.

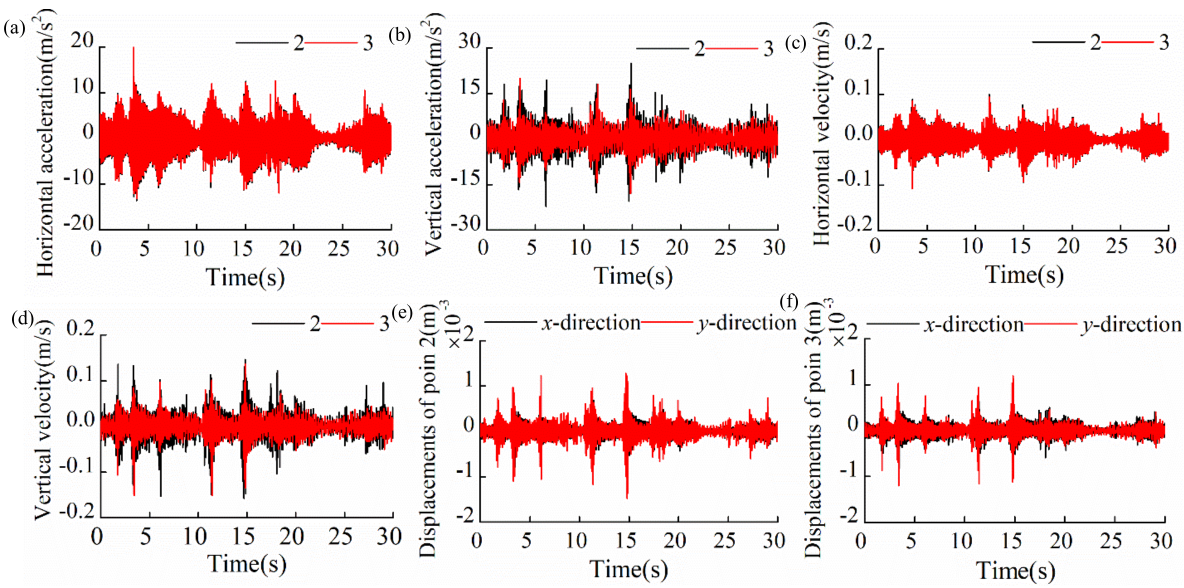

FIGURE 13. Testing results of dynamic characteristic with two co-rotating rotors coupled with a tensile-spring in a vibrating system.

comparison between the dynamic test results and the simulation results in a vibrating system are given in Table 5. The coupling unit with the stress state and unstressed state of the tensile-spring occuring periodically and alternately can be ensured the synchronous operation of the system. It can be seen that the horizontal acceleration of point P_2 is consistent

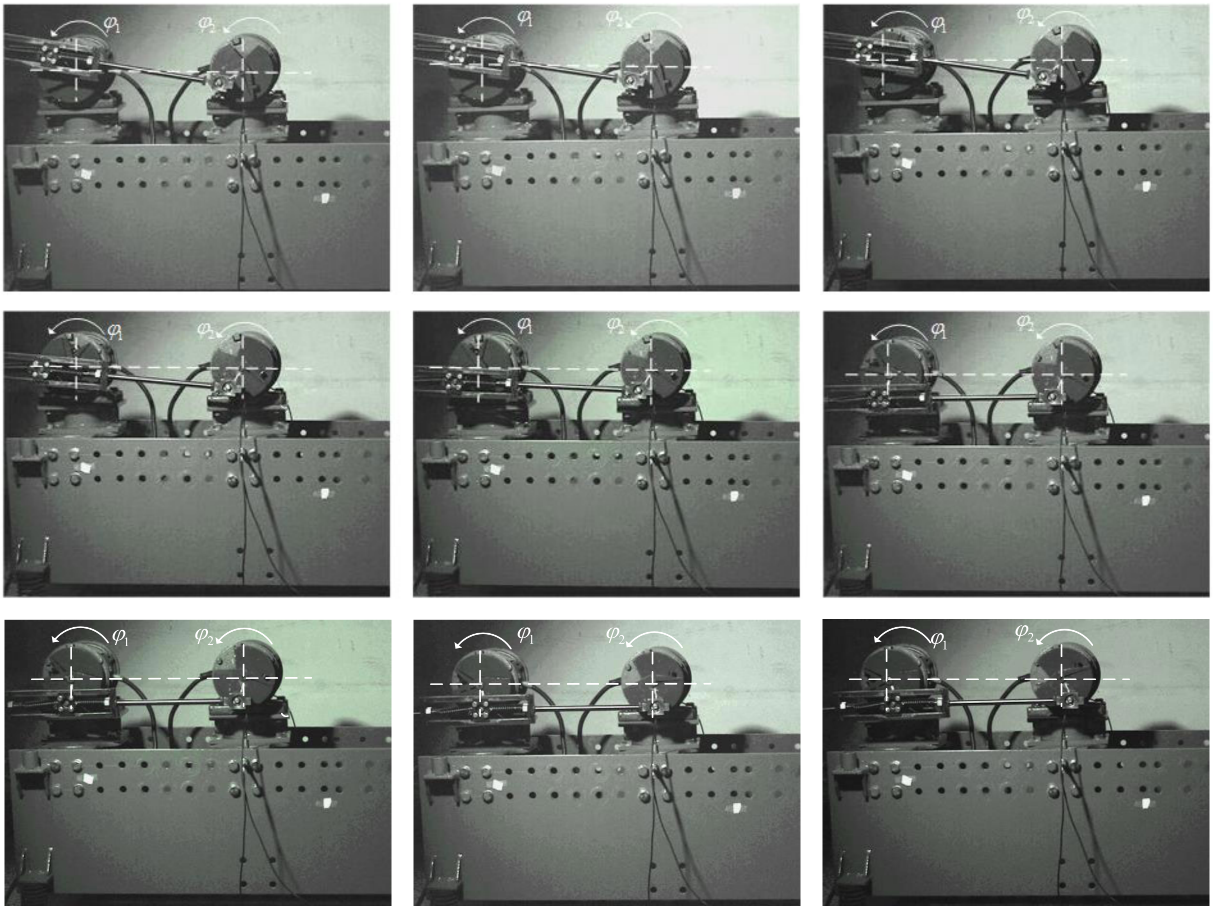

FIGURE 14. Phase difference with two co-rotating rotors coupled with nonlinear springs in a vibrating system.

TABLE 3. The comparison between the dynamic test results and the simulation results with two co-rotating rotors in a vibrating system.

	Results of dynamic testing		Results of dynamical simulation		Error value	
	x-direction	y-direction	x-direction	y-direction	x-direction	y-direction
Measuring point P_1	0.0019	0.0033	0.0015	0.0039	21.1%	15.3%
Measuring point P_2	0.0018	0.0019	0.0015	0.002	16.7%	5%
Measuring point P_3	0.0018	0.0016	0.0015	0.0013	16.7%	18.7%
Measuring point P_4	0.0019	0.0028	0.0015	0.003	21.1%	6.7%

TABLE 4. The comparison between the testing value and the simulation value of phase difference with two co-rotating rotors in a vibrating system.

	The result of the indirect experimental tests	The result of computer simulation	Error value
Steady phase difference 2α (rad)	-205.9° $\triangleq$ 2.69	3.03	11.2%

with point P_3, and the amplitude of acceleration is equal to 20 m/s^2, as shown in Figure 15(a). However, those vertical acceleration in numerical value was different, the acceleration amplitude of point P_2 and P_3 are 44.1 m/s^2 and 19.3 m/s^2, respectively, as shown in Fig 13(b). From Figure 15(c)$\sim$(f), the displacement and velocity of point P_2 and P_3 in horizontal and vertical directions can be obtained. In addition, the corresponding electromagnetic coupling model with two co-rotating rotors coupled with nonlinear springs is also carried out for obtaining its displacement amplitudes by computer simulations. From Table 5, Comparing the dynamic test results and the simulation results, it is easy to see that the error of magnitudes of point P_2 and P_3 is within 30%, and the computer simulations results are proved to be in good agreement with the testing results. The motion trajectories of point P_2 and P_3 in the rigid frame are elliptically, as shown in Figure 15(g). Owing to considerable differences of the displacement amplitudes of point P_2 and P_3 in vertical direction, the ovality and the direction of long axis in the motion trajectories are different.

From Figure 16, the transiently state of two co-rotating rotors coupled with a tensile-spring in a vibrating system are obtained by the high-speed camera. During the running process of the steady-state, the tensile-spring suffering from the stress state and unstressed state can ensure the synchronous

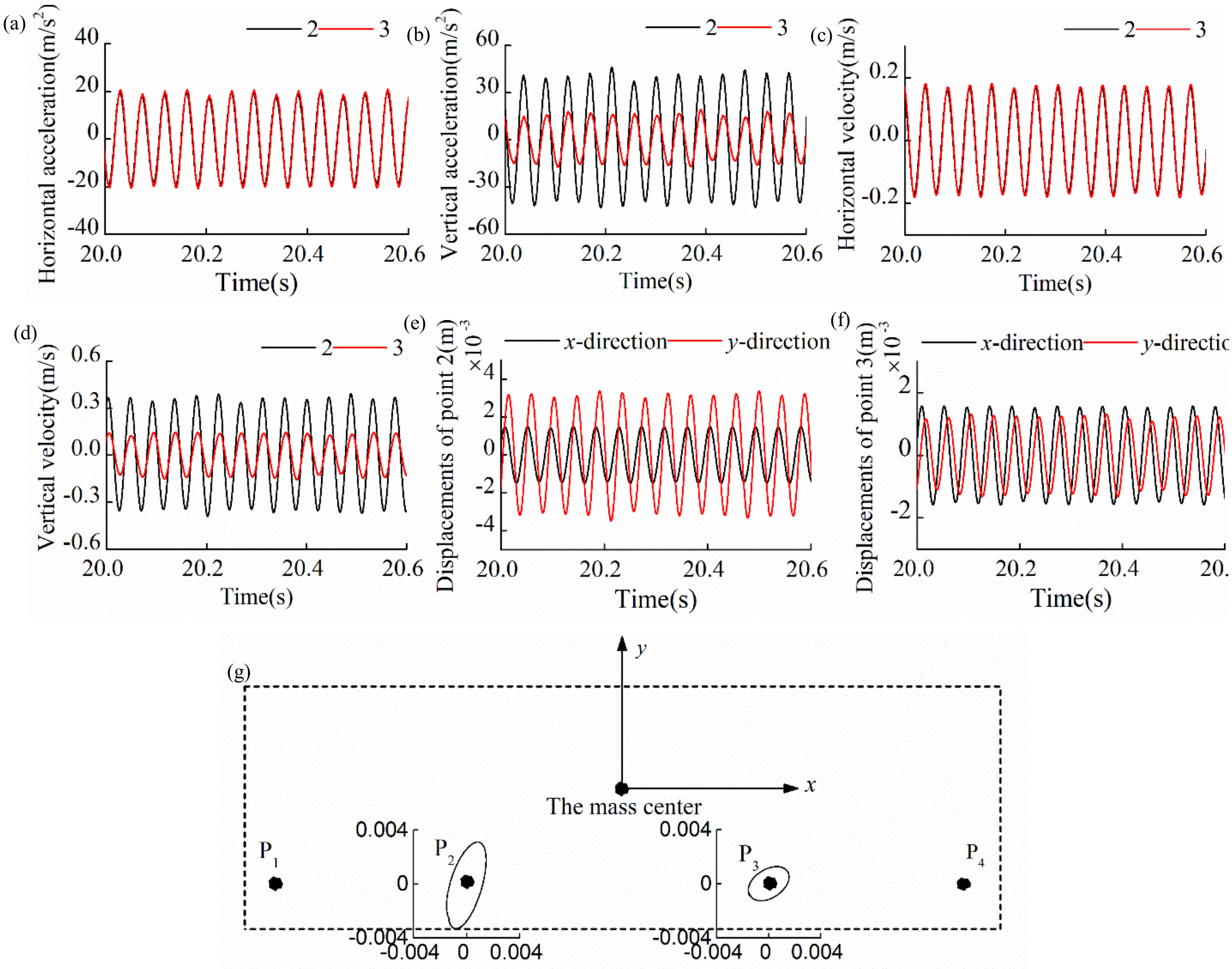

FIGURE 15. Testing results of dynamic characteristic with two co-rotating rotors coupled with a tensile-spring in a vibrating system: (a) Horizontal accelerations of the measuring point; (b) Vertical accelerations of the measuring point; (c) Horizontal velocity of the measuring point3; (d) Vertical velocity of the measuring point; (e) Displacements of the point 2; (f) Displacements of the point 3; (g) Motion trail of the measuring point in *xoy* plane.

TABLE 5. The comparison between the dynamic test results and the simulation results with two co-rotating rotors coupled with a tensile-spring in a vibrating system.

	The results of dynamic testing		The results of dynamical simulation		Error value	
	x-direction	y-direction	x-direction	y-direction	x-direction	y-direction
Measuring point P_2	0.0017	0.0016	0.0021	0.0015	19%	23.8%
Measuring point P_3	0.0032	0.0014	0.0027	0.0018	15.6%	22.2%

TABLE 6. The comparison between the testing value and the simulation value of phase difference with two co-rotating rotors coupled with a tensile-spring in a vibrating system.

	Result of the indirect experimental tests	Result of computer simulation	Error value
Steady phase difference 2α (rad)	$0.67° \triangleq 0.012$	$0.75° \triangleq 0.013$	7.7%

operation of the system, and two exciters are rotating with the same frequency. It is evident that the instantaneous phase relationship (2α) of two exciters during the synchronous state is nearly 0.012[rad]($-0.67°$). The simulation results of phase difference of two exciters were proven to be in good agreement with its testing result in Table 6 (the phase difference of two exciters in the simulation is close to 0.75°), and the error is 7.7%.

V. ERROR ANALYSIS

According to the above comparisons of the dynamic testing results, synchronous testing results and simulations results, resulting in a certain error between those are summarized as follows:

(1) In the process of the theory model and simulation, owing to that the mass of two exciters are far less distinct

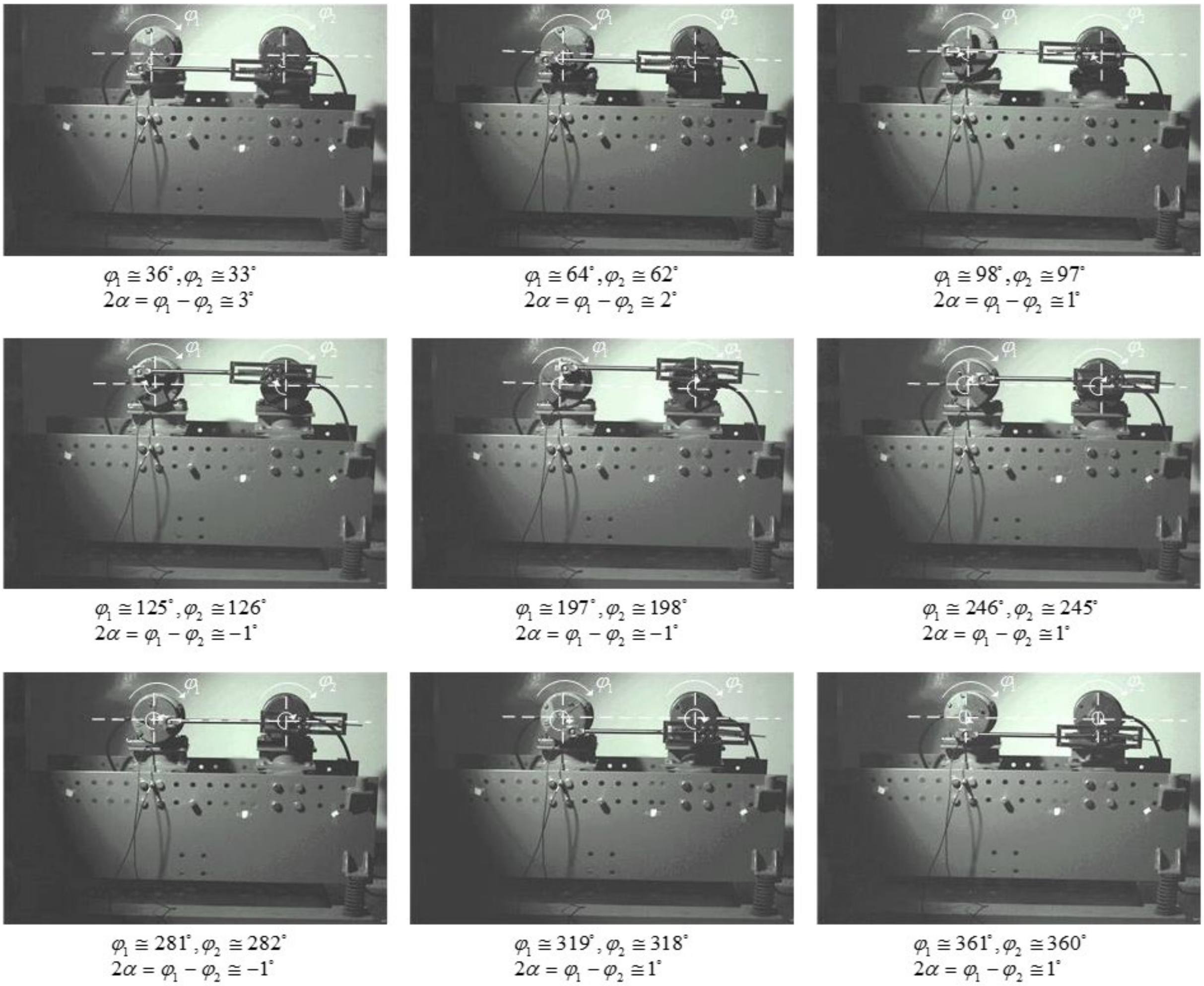

FIGURE 16. Phase difference with two co-rotating rotors coupled with a tensile-spring in a vibrating system.

than the rigid body and the oscillating angle of the mass center, the inertia coupling stemming from asymmetry of the two exciters can be ignored. Additionally, the differences among the manufacturing process of exciters result in the inconsistent performance parameters in the same type. However, when the vibrating system operates at the steady-state, the action of the nonlinear spring is to overcome the difference of residual torques, and the difference of residual torques between exciter 1 and 2 will not be equal to zero in engineering applications, which have caused some errors between the results obtained by theory and tests.

(2) After the processing and assembling of experimental prototype there still remains an error; The location of those measuring-point in rigid frame is not consistent with that chose by the computer simulation; There will be differences among those springs proposed in the model, and its stiffness coefficients are obtained by a quasilinearization method and are, hence, approximate value; There are differences on a signal transmission of sensors in different channel, and between the damping of system in the simulation and the actual prototype model. All of those caused the difference between the dynamic test results and the simulation results.

(3) During synchronous testing of the system, a high-speed camera is not completely perpendicular to the viewing angle of eccentric blocks, and the transiently state of two exciters are simultaneously obtained by photos measuring approximatively. In addition, the mass center of the experimental prototype is not fully overlap with the simulation mode. For these reasons, some error exists between the testing results and the simulation results.

VI. CONCLUSION

According to above discussions, the following conclusions should be stressed:

The theoretical derivations including conditions of implementing the synchronization and ensuring stable operation of the vibrating system are obtained by using the average method. In view of formulas equations (1), some computer simulations were carried out to explore the coupling characteristics of the system by means of the Runge–Kutta algorithm with adaptive control. Besides, an experimental prototype consisting of synchronous tests and dynamic characteristic tests is constructed to prove the correctness of the simulation analysis and theoretical derivations. And those error analysis among the dynamic testing results, synchronous testing results and simulation results are discussed. The simulations and experiments demonstrate that the nonlinear springs can overcome the difference of residual torques of the two motors to realize the synchronization of zero phase difference under the condition of in-phase difference between two exciters. The vibrating system has severe nonlinearities when two co-rotating rotors installed with two serial springs on which there is clearance, and two exciters can't rotate with the same velocity. One exciter is in good operation, and the other exciter is swing from side to side. In addition, two co-rotating eccentric rotors coupled with nonlinear springs can easily proposed to implement in-phase synchronization and meet the requirements of the strongly exciting force in engineering.

APPENDIX

$$\rho_1 = \eta_{12} + \frac{1}{2}\eta_{12}^2 W_{c1} \tag{A-1}$$

$$\rho_2 = 1 + \frac{1}{2}W_{c2} \tag{A-2}$$

$$k_1 = \eta_{12}^2 W_{s1} + \frac{k_{e1}}{m_2 r^2 \omega_m^2} + \frac{f_1}{m_2 r^2 \omega_m} \tag{A-3}$$

$$k_2 = W_{s2} + \frac{k_{e2}}{m_2 r^2 \omega_m^2} + \frac{f_2}{m_2 r^2 \omega_m} \tag{A-4}$$

$$\begin{aligned}\mu_1 = {} & \frac{T_{e01}}{m_2 r^2 \omega_m} - \frac{f_1}{m_2 r^2} - \frac{1}{2}\eta_{12}^2 \omega_m W_{s1} \\ & + \frac{T_{e02}}{m_2 r^2 \omega_m} - \frac{f_2}{m_2 r^2} - \frac{1}{2}\omega_m W_{s2} - \omega_m W_c \cos(2\alpha + \theta_c)\end{aligned} \tag{A-5}$$

$$\begin{aligned}\mu_2 = {} & \frac{T_{e01}}{m_2 r^2 \omega_m} - \frac{f_1}{m_2 r^2} - \frac{1}{2}\eta_{12}^2 \omega_m W_{s1} - \frac{T_{e02}}{m_2 r^2 \omega_m} \\ & + \frac{f_2}{m_2 r^2} + \frac{1}{2}\omega_m W_{s2} - \omega_m W_s \sin(2\alpha - \theta_s) \\ & - \frac{k a^2 \sin(2\alpha)}{m_2 r^2 \omega_m}\end{aligned} \tag{A-6}$$

$$W_{c1} = r_m \left[\mu_x \cos\gamma_x + \mu_y \cos\gamma_y + \mu_\psi r_{l1}^2 \cos\gamma_\psi\right] \tag{A-7}$$

$$W_{s1} = r_m \left[\mu_x \sin\gamma_x + \mu_y \sin\gamma_y + \mu_\psi r_{l1}^2 \sin\gamma_\psi\right] \tag{A-8}$$

$$W_{c2} = r_m \left[\mu_x \cos\gamma_x + \mu_y \cos\gamma_y + \mu_\psi r_{l2}^2 \cos\gamma_\psi\right] \tag{A-9}$$

$$W_{s2} = r_m \left[\mu_x \sin\gamma_x + \mu_y \sin\gamma_y + \mu_\psi r_{l2}^2 \sin\gamma_\psi\right] \tag{A-10}$$

$$\begin{aligned}a_s = {} & \mu_x \cos\gamma_x + \mu_y \cos\gamma_y \\ & + \mu_\psi r_{l1} r_{l2} \cos(\beta_1 - \beta_2) \cos\gamma_\psi\end{aligned} \tag{A-11}$$

$$b_s = \mu_\psi r_{l1} r_{l2} \sin(\beta_2 - \beta_1) \cos\gamma_\psi \tag{A-12}$$

$$\begin{aligned}a_c = {} & \mu_x \sin\gamma_x + \mu_y \sin\gamma_y \\ & + \mu_\psi r_{l1} r_{l2} \cos(\beta_1 - \beta_2) \sin\gamma_\psi\end{aligned} \tag{A-13}$$

$$b_c = \mu_\psi r_{l1} r_{l2} \sin(\beta_1 - \beta_2) \sin\gamma_\psi \tag{A-14}$$

$$W_s = \eta_{12} r_m \sqrt{a_s^2 + b_s^2} \tag{A-15}$$

$$\theta_s = \begin{cases} \arctan\dfrac{b_s}{a_s}, & a_s \geq 0 \\ \pi + \arctan\dfrac{b_s}{a_s}, & a_s < 0 \end{cases} \tag{A-16}$$

$$W_c = \eta_{12} r_m \sqrt{a_c^2 + b_c^2} \tag{A-17}$$

$$\theta_c = \begin{cases} \arctan\dfrac{b_c}{a_c}, & a_c \geq 0 \\ \pi + \arctan\dfrac{b_c}{a_c}, & a_c < 0 \end{cases} \tag{A-18}$$

REFERENCES

[1] I. I. Blekhman, *Synchronization in Science and Technology*. New York, NY, USA: ASME, 1988.

[2] I. I. Blekhman, *Vibrational Mechanics*. 2002, p. 509. [Online]. Available: https://www.worldscientific.com/worldscibooks/10.1142/4116

[3] B. Wen and C. Zhao, *Vibratory Synchronization and Controlled Synchronization in Engineering*. Beijing, China: Science Press, 2009.

[4] B. Wen, J. Fan, and C. Zhao, *Synchronization and Controled Sychronization in Engineering*. Beijing, China: Science Press, 2009.

[5] C. Zhao, H. Zhu, R. Wang, and B. Wen, "Synchronization of two non-identical coupled exciters in a non-resonant vibrating system of linear Motion. Part I: Theoretical analysis," *Shock Vib.*, vol. 16, no. 5, pp. 505–515, 2009.

[6] X.-L. Zhang, B.-C. Wen, and C.-Y. Zhao, "Synchronization of three homodromy coupled exciters in a non-resonant vibrating system of plane motion," *Acta Mechanica Sinica*, vol. 28, no. 5, pp. 1424–1435, Oct. 2012.

[7] X. Zhang, B. Wen, and C. Zhao, "Theoretical, numerical and experimental study on synchronization of three identical exciters in a vibrating system," *Chin. J. Mech. Eng.*, vol. 26, no. 4, pp. 746–757, Jul. 2013.

[8] X. Zhang, B. Wen, and C. Zhao, "Synchronization of three non-identical coupled exciters with the same rotating directions in a far-resonant vibrating system," *J. Sound Vib.*, vol. 332, no. 9, pp. 2300–2317, Apr. 2013.

[9] X. Zhang, B. Wen, and C. Zhao, "Experimental investigation on synchronization of three co-rotating non-identical coupled exciters driven by three motors," *J. Sound Vib.*, vol. 333, no. 13, pp. 2898–2908, Jun. 2014.

[10] X. Kong, X. Chen, J. Dou, X. Zhang, and B. Wen, "Controlled synchronization of two nonidentical homodromy coupling exciters driven by inductor motors in a vibratory system," *Proc. Ins. Mech. Eng. C, J. Mech. Eng. Sci.*, vol. 230, no. 17, pp. 3040–3054, Oct. 2016.

[11] X. Kong, X. Zhang, X. Chen, B. Wen, and B. Wang, "Synchronization analysis and control of three eccentric rotors in a vibrating system using adaptive sliding mode control algorithm," *Mech. Syst. Signal Process.*, vols. 72–73, pp. 432–450, May 2016.

[12] X. Kong, X. Zhang, X. Chen, B. Wen, and B. Wang, "Phase and speed synchronization control of four eccentric rotors driven by induction motors in a linear vibratory feeder with unknown time-varying load torques using adaptive sliding mode control algorithm," *J. Sound Vib.*, vol. 370, pp. 23–42, May 2016.

[13] X. Chen, X. Kong, X. Zhang, L. Li, and B. Wen, "On the synchronization of two eccentric rotors with common rotational axis: Theory and experiment," *Shock Vib.*, vol. 2016, pp. 1–14, 2016.

[14] X. Chen, X. Kong, Y. Liu, and B. Wen, "Synchronization and coupling dynamic characteristics of a dual-rotors exciter," *J. Vibroeng.*, vol. 18, no. 5, pp. 3318–3328, Aug. 2016.

[15] X. Chen, X. Kong, J. Dou, Y. Liu, and B. Wen, "Numerical and experimental investigation on self-synchronization of two eccentric rotors in the vibration system," *J. Vibroeng.*, vol. 18, no. 2, pp. 744–758, Mar. 2016.

[16] P. Fang, Y. Hou, and M. Du, "Synchronization behavior of triple-rotor-pendula system in a dual-super-far resonance system," *Proc. Inst. Mech. Eng., C, J. Mech. Eng. Sci.*, vol. 233, no. 5, pp. 1620–1640, Mar. 2019.

[17] Y. Hou and P. Fang, "Investigation for synchronization of a rotor-pendulum system considering the multi-DOF vibration," *Shock Vib.*, vol. 2016, pp. 1–22, 2016.

[18] P. Fang, Q. Yang, Y. Hou, and Y. Chen, "Theoretical study on self-synchronization of two homodromy rotors coupled with a pendulum rod in a far-resonant vibrating system," *J. Vibroeng.*, vol. 16, no. 5, pp. 2188–2204, Aug. 2014.

[19] Y. Hou, M. Du, and L. Wang, "Investigation for synchronization of two co-rotating rotors installed with nonlinear springs in a non-resonance system," *Adv. Mech. Eng.*, vol. 11, no. 3, Mar. 2019, Art. no. 168781401983411.

MINGJUN DU was born in 1991. He received the M.E. degree in mechatronics engineering from Southwest Petroleum University, China, in 2017, where he is currently pursuing the Ph.D. degree in mechanical engineering. His research interests include synchronization theory, vibration utilization and control engineering, and nonlinear vibrations in engineering.

YONGJUN HOU was born in 1967. He received the Ph.D. degree in mechanics from Southwest Petroleum University, China, in 2002. He is currently a Professor with the School of Mechanical Engineering, Southwest Petroleum University, where he leads the research group working on vibration utilizing engineering, synchronization theory of vibrating systems, nonlinear vibrations in engineering, rotors dynamics, and comprehensive design theory. He has published over 80 scientific articles in journals and conferences at home and abroad.

CHENG YU received the M.E. degree in mechatronics engineering from Southwest Petroleum University, China, in 2017, where she is currently pursuing the Ph.D. degree in mechanical engineering. At the same time, she has taught in Chengdu Technological University. Her research interests include natural gas hydrate, fluid-solid coupling, and computer simulation.

WEI WANG was born in 1993. He is currently pursuing the master's degree in mechanical engineering with Southwest Petroleum University, China. His main research interests include mechanical engineering and robot structure control.

DUYU HOU received the B.S. degree in mechanics from the Sichuan University Jinjiang College, China, in 2017. He is currently pursuing the M.S. degree with the School of Mechanical Engineering, Southwest Petroleum University, China. His research interests include dynamics of multiexciter systems and nonlinear systems, and dynamics of synchronizing systems.

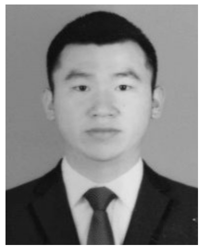

GUANG XIONG is currently pursuing the M.S. degree with Southwest Petroleum University, China. His research interests include vibration in mechanics, nonlinear systems, and numerical simulation.